

Polyvalent Cations as Permeant Probes of MIC and TRPM7 Pores

Hubert H. Kerschbaum,^{*†} J. Ashot Kozak,^{*} and Michael D. Cahalan^{*}

^{*}Department of Physiology and Biophysics, University of California, Irvine, California 92697-4561 USA; and [†]Department of Molecular Neurobiology and Cellular Physiology, Institute for Zoology, University of Salzburg, A-5020 Salzburg, Austria

ABSTRACT Recent studies in Jurkat T cells and in rat basophilic leukemia cells revealed an Mg^{2+} -inhibited cation (MIC) channel that has electrophysiological properties similar to TRPM7. Eyring rate model expressed exogenously in mammalian cells. Here we compare the characteristics of several polyvalent cations and Mg^{2+} to block monovalent MIC current from the outside. Putrescine, spermidine, spermine, PhTX-343 (a derivative of the naturally occurring polyamine toxin philanthotoxin), and Mg^{2+} each blocked in a dose- and voltage-dependent manner, indicating a blocking site within the electric field of the ion channel. Spermine and the relatively bulky PhTX-343 exhibited voltage dependence steeper than that expected for the number of charges on the molecule. Polyamines and Mg^{2+} are permeant blockers, as judged by relief of block at strongly negative membrane potentials. Intracellular dialysis with spermine (300 μ M) had no effect, indicating an asymmetrical pore. At the single-channel level, spermine and Mg^{2+} induced flickery block of 40-pS single channels. I/V characteristics and polyamine block are similar in expressed TRPM7 and in native MIC currents, consistent with the conclusion that native MIC channels are composed of TRPM7 subunits. An Eyring rate model is developed to account for I/V characteristics and block of MIC channels by polyvalent cations from the outside.

INTRODUCTION

TRPM7, a member of the long TRP family, produces an outwardly rectifying nonselective cation channel when expressed heterologously in mammalian cells (Runnels et al., 2001; Nadler et al., 2001). The human T-cell line, Jurkat, human peripheral T cells, and rat basophilic leukemia (RBL) cells possess a native current with similar properties. Under conditions of divalent-free external solution and Mg^{2+} -free internal solution, a large monovalent current gradually develops during whole cell dialysis in these cells (Kerschbaum and Cahalan, 1998, 1999; Fomina et al., 2000; Braun et al., 2001). The monovalent current consists of the summed activity of tens to hundreds of \sim 40 pS channels per cell, each opening to a state of a high open probability ($P_o > 0.9$). Using organic monovalent cations of varying size, we estimated the pore diameter of this nonselective cation channel to be \sim 6 Å (Kerschbaum and Cahalan, 1998). Originally, it was proposed that the Ca^{2+} release-activated Ca^{2+} (CRAC) channel transforms into a nonselective cation channel upon removal of external divalent cations (Kerschbaum and Cahalan, 1998, 1999). Recently, this view was revised as a result of electrophysiological and molecular biological findings that show differences in the pharmacology, store dependence, and ion selectivity of the divalent and monovalent currents (Hermosura et al. 2002; Prakriya and Lewis, 2002; Kozak et al., 2002). The properties of the native nonselective cation current, named either MagNum (for magnesium-nucleotide-inhibited metal) (Nadler et al., 2001) or MIC (Mg^{2+} -inhibited cation) (Prakriya and Lewis,

2002) for their inhibition by Mg^{2+} or Mg^{2+} nucleotides, match well with cloned and expressed TRPM7 channels (Nadler et al., 2001; Runnels et al., 2001). The most striking electrophysiological similarities between MIC channels and TRPM7 channels are the I/V shape, inhibition by intracellular Mg^{2+} ion, and permeability to several monovalent and divalent cations (Runnels et al., 2001; Nadler et al., 2001; Prakriya and Lewis, 2002; Kozak et al., 2002). Molecular biological experiments revealed expression of TRPM7 mRNA in Jurkat cells and RBL cells (Nadler et al., 2001).

Although the electrophysiological properties of both MIC and CRAC channels have been studied in some detail, the pharmacology of these channels is still in a premature state. CRAC and MIC are both inhibited by external Ni^{2+} , La^{3+} , and Gd^{3+} (Runnels et al., 2001; Hermosura et al., 2002). CRAC channels are blocked reversibly by the imidazole antimycotic compound SKF 96365, whereas MIC channels are either insensitive to SKF 96365 in Jurkat cells (Prakriya and Lewis, 2002), or irreversibly inhibited in RBL cells (Kozak et al., 2002). We recently showed that spermine can distinguish MIC from CRAC channels, blocking monovalent MIC current selectively at micromolar concentrations (Kozak et al., 2002).

Blockers have been used frequently, along with the ion selectivity profile and gating characteristics, to establish a biophysical fingerprint for comparing native channels with those in expression systems. For example, a detailed comparison of blocker potencies and other biophysical characteristics led to the identification of Kv1.3 and IKCa1 as the voltage-gated and Ca^{2+} -activated K^+ channels, respectively, in human T cells (reviewed in Cahalan et al., 2001). One goal of the present study was to compare the pharmacological profile of native MIC and expressed TRPM7 channels using polyamines and other polyvalent

Submitted September 26, 2002, and accepted for publication November 21, 2002.

Address reprint requests to Michael D. Cahalan, Dept. of Physiology and Biophysics, University of California, Irvine, CA 92697-4561. Tel.: 949-824-7776; Fax: 949-824-3143; E-mail: mcahalana@uci.edu.

© 2003 by the Biophysical Society

0006-3495/03/04/2293/13 \$2.00

cations as probes. Here, we compare the action of external Mg^{2+} with several polyamines: putrescine, spermidine, and spermine that are ubiquitous cytoplasmic metabolites; and philanthotoxin-343 (PhTX-343), a synthetic polyamine analog of the toxin present in the venom of the wasp *Philanthus triangulum* (Eldefrawi et al., 1988). Analysis of the relief of block at negative potentials suggests a permeant block mechanism and provides an independent estimate of the pore diameter for comparison with previous work on bulky permeant ions (Kerschbaum and Cahalan, 1998). Polyamines specifically blocked monovalent current through native MIC channels and expressed TRPM7 channels. We provide an empirical description of ion permeation and block in terms of an Eyring rate theory model.

METHODS

Cell culture

The human leukemic T-cell line, Jurkat E6-1, was cultured in RPMI 1640 with 10% fetal bovine serum (FBS), 1 mM glutamine, and 25 mM HEPES. RBL-2H3 cells were grown in EMEM with 10% FBS and Chinese hamster ovary (CHO)-K1 cells were grown in F-12K and 10% FBS. All cell lines were grown in a 5% CO_2 incubator at 37°C. The cells were passaged every two days.

Electrophysiological recordings from Jurkat, RBL, and CHO cells

Macroscopic and single-channel currents were recorded in the whole-cell recording configurations (Hamill et al., 1981) at room temperature using an EPC-9 patch clamp amplifier (HEKA Elektronik, Lambrecht, Germany). Data were acquired and analyzed using Pulse/Pulsefit (v. 8.11) (HEKA), Igor Pro (v. 3.1.2) (WaveMetrics, Lake Oswego, OR), and Microcal Origin (v. 6) (Microcal Software, Northampton, MA) software.

Pipettes were pulled from soft glass capillaries (Becton-Dickinson, Parsippany, NJ), coated with Sylgard (Dow Corning, Midland, MI), and fire-polished to a resistance of 2–5 M Ω when filled with internal solutions. The glass coverslip chambers used for Jurkat T cell recordings were coated with poly-L-lysine (1 mg/ml) to improve adherence to the dish. Currents were sampled at 5–25 kHz and digitally filtered offline at 1 kHz. The membrane potential was held at 0 mV and currents were studied during 200-msec voltage ramps from –120 mV to +40 mV or during voltage steps from 0 mV to –120 mV. To measure the amplitude of the monovalent current through MIC channels at a given potential more accurately, we applied voltage steps. Voltage ramp or step stimuli were delivered at 1 Hz. Leak currents before activation of MIC channels were averaged and subtracted from subsequent current records. Slow and fast capacitative transients were canceled by the compensation circuitry of the EPC-9. Series resistance (~10 M Ω) was not compensated. Quantitative analysis of block was restricted to cells and membrane potentials at which control currents were <0.5 nA and errors due to uncompensated series resistance negligible. Cells were superfused with various solutions by bath exchange. Local solution exchanges were performed via puffer pipettes, as described previously (Lepple-Wienhues and Cahalan, 1996). Durations of open and closed events were estimated from idealized single channel data using TAC software (Bruxton; Seattle, WA). Currents were sampled at a rate of 5–10 kHz and filtered with a Gaussian filter at 1 kHz, resulting in a rise time of 330 μ s. Channel opening and closing events were detected using a half-amplitude threshold paradigm, allowing detection of events of ~200 μ s duration. Data were not corrected for missed events. Idealized current traces were used to

generate dwell-time histograms and estimated open and closed durations by fitting the data to a probability density function. At moderate concentrations of polyvalent cations, clear opening and closing events were resolved. Time constants for open and closed times, τ_{open} and τ_{closed} , respectively, were calculated from probability density functions assuming a single exponential distribution. Channel open probability (P_o) was calculated from an all-points amplitude histogram, or from the ratio $\tau_{open}/(\tau_{open} + \tau_{closed})$; both methods yielded similar values. Calculation of $K_{1/2}$, the concentration of blocker that reduced current amplitude by half, and the Boltzmann term k representing the steepness of voltage-dependent block, were performed with Igor Pro and Microcal Origin software. Ted Begenisich kindly provided the program that we used to calculate current-voltage relations from a four-barrier, three-site Eyring rate model.

Solutions

Jurkat T lymphocytes

Divalent-free external solution contained (mM): 150 Na^+ methane sulfonate or Cs^+ methane sulfonate, 10 HEDTA, and 10 HEPES, pH 7.2. $MgCl_2$ was added to the external solution to achieve the desired external free Mg^{2+} as computed with MaxChelator (Bers et al., 1994). The pipette solution contained (mM): 150 Cs^+ aspartate or Na^+ aspartate, 10 Cs^+ -HEPES or Na^+ -HEPES, 12 BAPTA, and 0.9 $CaCl_2$, pH 7.2 titrated with CsOH or NaOH. All chemicals were purchased from Sigma (St Louis, MO).

RBL and CHO cells

The Ca^{2+} external solution contained (mM): 2 $CaCl_2$, 167 Na^+ aspartate, 2 Cs^+ methanesulfonate, and 10 HEPES, pH 7.3 titrated with NaOH. The divalent-free external solution consisted of 154 Cs^+ aspartate, 5 NaCl, 10 HEDTA, 2 Cs^+ methanesulfonate, and 10 HEPES, pH 7.3 titrated with CsOH. The internal solution contained: 130 Cs^+ glutamate, 8 NaCl, 0.9 $CaCl_2$, 12 EGTA, and 10 HEPES, pH 7.3 titrated with CsOH. Spermine hydrochloride (Calbiochem, La Jolla, CA) was added to the divalent-free external solution.

Expression of TRPM7 in CHO-K1 cells

CHO cells were grown in six-well plates and transiently transfected with the mouse TRPM7 clone in the pTracerCMV2 vector using the Effectene transfection kit (Qiagen, Valencia, CA) according to the manufacturer's procedure. The cells were replated on glass coverslips 24 h before electrophysiological recordings. Recordings were made 3–4 days after transfection. The transfected cells were visualized by green fluorescent protein fluorescence. To compare spermine block of the expressed TRPM7 current to the native MIC current in RBL cells, identical ramp protocols were applied (from –120 mV to +85 mV, 211 ms duration, applied at 0.5 Hz). Upon full development of MIC current in Ca^{2+} -containing external solution, the external solution was switched to divalent-free Cs^+ -HEDTA solution and spermine added.

RESULTS

External polyamines block monovalent current through MIC channels

Monovalent current through MIC channels was activated by dialysis of the cell with Mg^{2+} -free internal solution during exposure to divalent-free external solution. We initially compared the potency of three naturally occurring cytoplasmic polyamines—putrescine, spermidine, and spermine—to

block Na^+ current through MIC channels when applied from the outside. Fig. 1 shows the molecular structures of polyamines used in this paper. Qualitatively, these compounds behaved similarly, each producing a voltage-dependent block with varying potencies in the sequence: spermine > spermidine > putrescine. Block during exposure and unblock after wash were completed within 1 s (Fig. 2, *A*, *C*, and *E*). Inspection of *I/V* curves in Fig. 2, *B*, *D*, and *F*, shows that each of the three polyamines blocked in a voltage-dependent manner with maximal sensitivity near -40 mV, whereas at more depolarized or hyperpolarized potentials the block was less potent. The relief of block at potentials more positive than -40 mV is consistent with a binding site within the membrane electric field. At these depolarized voltages the positively charged polyamine molecule would be repelled outward away from the binding site. We interpret the relief of block at hyperpolarized potentials by postulating that polyamines are permeant blockers that can also exit the channel toward the cytoplasm, drawn inside by the electric field at negative membrane potentials. Similar characteristics of permeant block (also termed punch-through) by polyamines have been seen in inward rectifier K^+ (K_{IR}) and cyclic nucleotide-gated (CNG) channels, in the voltage-gated Na^+ channel, and in glutamate receptor channels (Bähring et al., 1997; Araneda et al., 1999; Guo and Lu, 2000a,b; Huang and Moczydlowski, 2001). Our findings indicate that polyamines are fast blockers that can approach an externally accessible high-affinity binding site within the MIC channel and can pass through the channel driven by the electric field.

In several ion channels, polyamines block conductance in a voltage-dependent manner from the inside. Furthermore, Mg^{2+} inhibits MIC channels from the inside (Nadler et al., 2001; Prakriya and Lewis, 2002), although this inhibition is not voltage-dependent and may not involve direct interaction with the pore (Kozak et al., 2002). Tested from the inside by inclusion in the pipette solution, $300 \mu\text{M}$ spermine produced no effect on the development of MIC current or *I/V*

characteristics ($n = 10$ cells; data not shown). These experiments indicate that spermine, at >1000 times the effective outside dose, cannot readily access the high-affinity binding site from the cytoplasmic side of the plasma membrane and thus suggest an asymmetric pore.

To characterize external polyamine block further, we examined the action of PhTX-343. PhTX-343 blocks several other channel types, but because of its larger size (see structures in Fig. 1), does not exhibit permeant block (punch-through) in the K_{IR} and CNG-gated channels (Guo and Lu, 2000a,b). Extracellular application of PhTX-343 blocked monovalent MIC current in a voltage-dependent manner with relief of block at both depolarized and hyperpolarized potentials (Fig. 3). The potency and voltage dependence is similar to that seen with spermine. A quick way to assess the voltage dependence of block is to divide *I/V* curves in the presence of blocker by a control *I/V* curve with no blocker present. As seen in Fig. 3 *B*, the resultant *I/V* ratio reflects the fraction of unblocked channels at each potential during a voltage ramp; block by PhTX-343 is most potent at the minimum of this curve from near -50 to -70 mV, and relief of block can be clearly observed at relatively depolarized and hyperpolarized voltages.

Fast kinetics of block are a necessary prerequisite to determine equilibrium blocker dose-response relations and steady-state voltage dependence of block from data taken with voltage ramps. Fig. 4 examines the kinetics of MIC channel block and unblock by spermine and PhTX-343 on a millisecond timescale using a step protocol. At -40 mV, the current was reduced by $\sim 50\%$ and the residual current trace exhibits increased fluctuations noisy during exposure to spermine (Fig. 4 *A*). During the step to $+40$ mV, the monovalent outward current was hardly affected by spermine, indicating a rapid relief of block at positive potentials. Finally, upon stepping back to -40 mV, block was immediately restored on a timescale faster than the resolution of the recording (<1 ms). Fast block and unblock kinetics were also observed for spermidine and putrescine (data not shown). In contrast, PhTX-343 block was slower than spermine to equilibrate at -40 mV ($\tau = 11$ ms) (Fig. 4 *B*). We conclude that spermine and related cytoplasmic polyamines exhibit block and unblock kinetics that are faster than the millisecond timescale and cannot be resolved temporally using this step paradigm. The nearly instantaneous block and relief of block justifies the use of voltage ramps for analysis of dose-response relationships. The slower equilibration of block by PhTX-343 can distort the apparent voltage dependence obtained using voltage ramp stimuli.

Quantitatively, the MIC channel shows varying sensitivity to different polyamines. Fig. 5 illustrates dose-response relations determined by measuring fractional block at varying concentrations and fitting with the Langmuir adsorption isotherm for a bimolecular interaction. These results and other characteristics of block are compared in

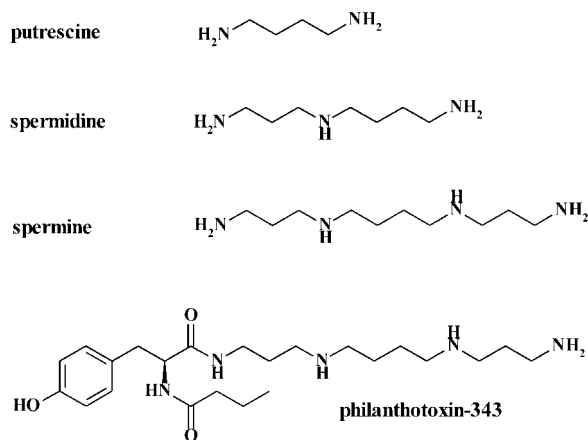


FIGURE 1 Structures: putrescine, spermidine, spermine, and PhTX-343.

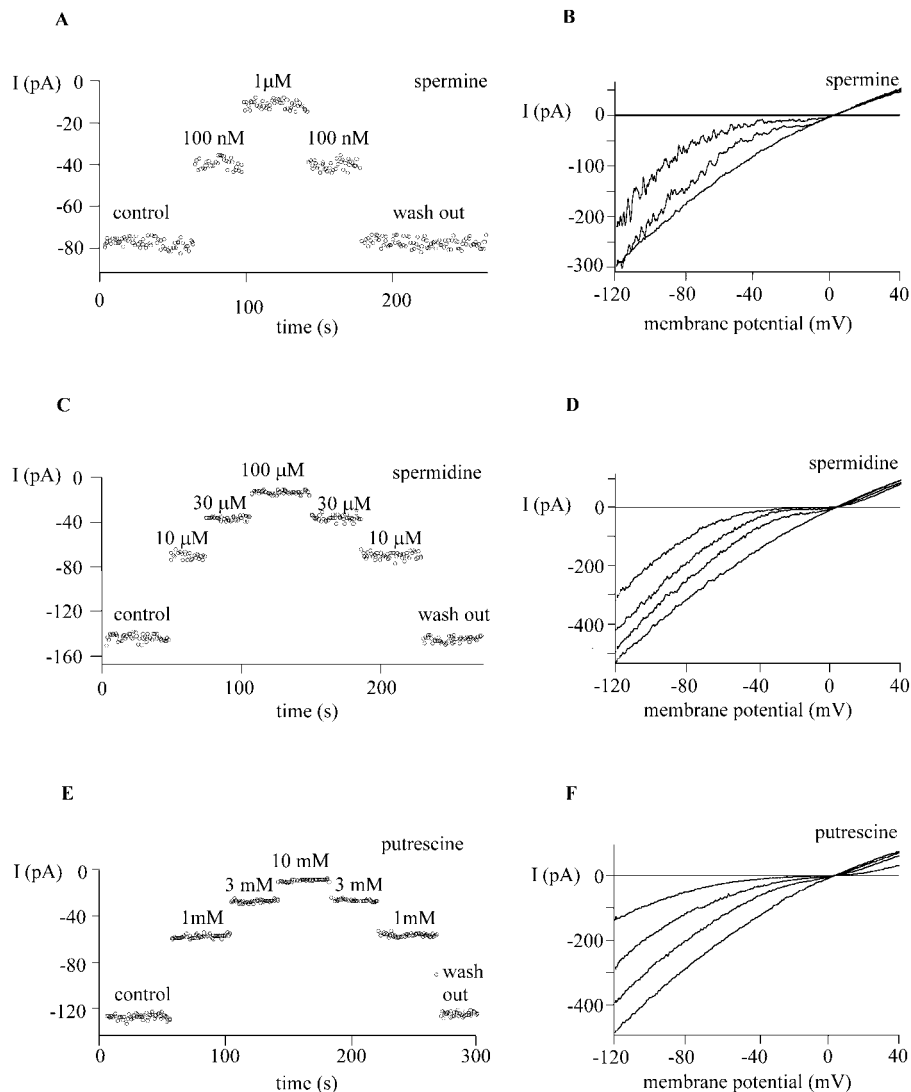


FIGURE 2 Spermine, spermidine, and putrescine inhibit MIC current reversibly. MIC channels were activated during whole-cell dialysis with Mg^{2+} -free internal solution during exposure to HEDTA-buffered divalent-free external solution. Inward current is carried by Na^+ and outward current by Cs^+ . After complete activation of the monovalent current, different concentrations of spermine (*A*, *B*), spermidine (*C*, *D*), and putrescine (*E*, *F*) were delivered to cells via a series of gravity-driven puffer pipettes. (*A*, *C*, and *E*) Time course of the monovalent current during exposure and washout of polyamines. Each data point represents the leak-subtracted current magnitude at -40 mV. (*B*, *D*, and *F*) Representative leak-subtracted current traces consisting of control and each of the concentrations in *A*, *C*, and *E*. Ramp currents, elicited by voltage ramps from -120 mV to $+40$ mV delivered at 1 Hz, reveal strong inhibition at moderately hyperpolarized potentials and weaker inhibition at depolarized membrane potentials by polyamines.

Table 1. Generally, the potency sequence parallels the number of positive charges. Evaluated at -40 mV, PhTX-343 and spermine each blocked MIC current with $K_{1/2}$ values of ~ 90 nM, followed by the trivalent spermidine at two log units lower potency, and then by the divalent putrescine again separated by two log units. As expected from visual inspection of the ramp currents before and after application of the polyamine, the $K_{1/2}$ value depends strongly on the membrane potential. Fig. 5, *B–D*, shows experimental data and corresponding Langmuir fits for spermine, spermidine, and putrescine block measured at -120 mV, -40 mV, and $+40$ mV. $K_{1/2}$ values were lowest at -40 mV and higher at depolarized or hyperpolarized potentials.

To examine the voltage dependence of polyamine block and punch-through in greater detail, we determined I/V ratio curves for each of the polyamines, as shown in Fig. 6 for spermine, spermidine, and putrescine, using the same procedure as described above for PhTX-343 (Fig. 3 *B*). The steepness of voltage-dependent block over the depolar-

ized range of potentials and relief of block at hyperpolarized potentials can be compared by fitting single Boltzmann functions, as illustrated by thin lines. Parameters for block and relief of block are summarized in Table 1. At depolarized potentials, relief of block reflects exit toward the outside and the steepness factor k (e-fold change in occupancy per mV change in voltage) parallels the number of charges; spermine and PhTX-343 are the steepest with an e-fold change per 5 mV. In principle, for the simple block model developed initially by Woodhull (1973), the steepness of block depends on the valence (z) of the blocker and the fraction of the electric field (δ from the outside) that the blocker has to traverse to reach its binding site. The steepness, expressed as the $z\delta$ product, increased from 1.6 for putrescine ($z = 2$), to 2.4 for spermidine ($z = 3$), to 5.2 for spermine ($z = 4$). For putrescine and spermidine, the result may indicate access from the outside to a binding site most of the way through the membrane, although the situation is likely to be more complex since polyamines have charges distributed along

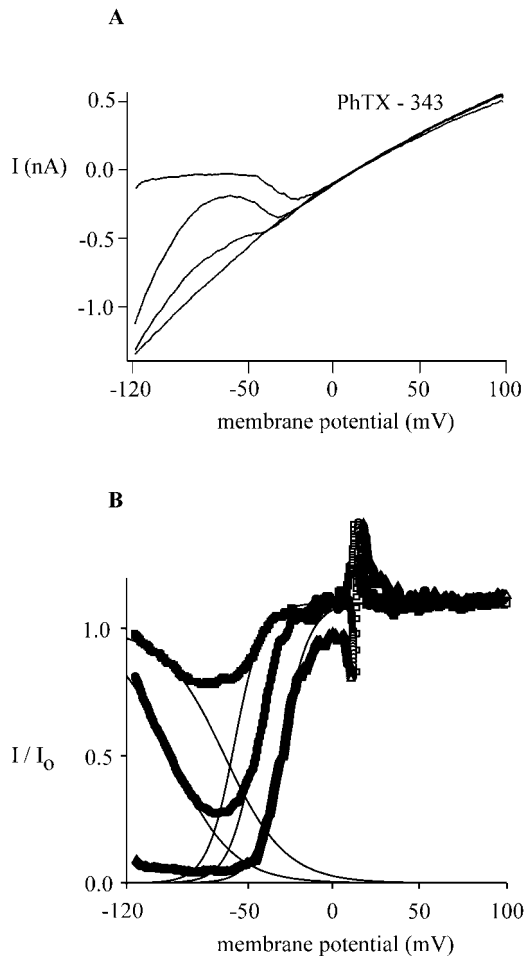


FIGURE 3 Concentration- and voltage-dependent block of leak-subtracted MIC current by PhTX-343. The cell was dialyzed with Mg^{2+} -free Na^+ -aspartate internal solution and exposed to HEDTA-buffered divalent-free external solution. Voltage ramps from -120 mV to $+100$ mV lasted 200 ms and were delivered every second. After maximal development of the monovalent current, the cell was exposed to PhTX-343. (A) Macroscopic I/V curves of MIC current in the absence and presence of 30 nM, 100 nM, and 1 μ M PhTX-343. Application of PhTX-343 reduced inward MIC current amplitudes preferentially, transforming MIC current from a mild to a strong inwardly rectifying current and leaving the amplitude of the outward current untouched. (B) Fraction of unblocked current obtained from A is plotted versus membrane potential. The current ratios indicate that PhTX-343 is a permeant blocker of MIC channels, forced through the pore by the strength of the electric field at very hyperpolarized membrane potentials. The solid lines between -120 mV and $+100$ mV represent a fit of the current ratio to a Boltzmann function: $I/I_0 = (-1/1 + \exp[V - V_{0.5}]/k) + 1$ for the voltage-dependent block, and $I/I_0 = (1/1 + \exp[V - V_{0.5}]/k)$ for the voltage-dependent relief of block, where I_0 is the current before and I the current after application of PhTX-343, V is the membrane potential, $V_{0.5}$ the membrane potential at which the current is blocked by 50%, and k is a slope factor representing the voltage dependence of the block. The slope factor, k , is $RT/z\delta F$, where z is the valence of the blocker and δ is the fraction of the membrane electric field. For the voltage-dependent block, $V_{0.5}$ values for 30, 100, and 1000 nM PhTX-343 are -58 , -45 , and -30 mV, respectively. The value of k did not change with PhTX-343 concentration and is 5.4 mV, corresponding to $z\delta = 4.6$. For the voltage-dependent relief of block, $V_{0.5}$ at 30 nM PhTX-343 is -96 mV, and -68 mV at 100 nM PhTX. The slope factor k is 17.6 mV, and $z\delta$ is 1.42.

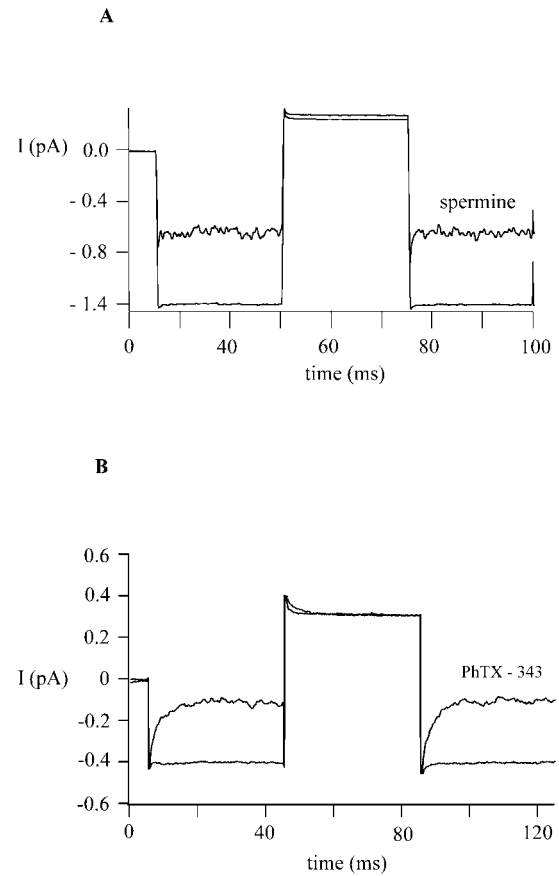


FIGURE 4 Fast block and unblock of MIC channels by spermine and PhTX-343. MIC channels were activated as described in Figs. 2 and 3. The membrane potential was stepped from -40 mV to $+40$ mV and the corresponding current recorded in the absence and presence of spermine (100 nM) (A) and PhTX-343 (100 nM) (B). Both polyamines are potent blockers at -40 mV but fail to reduce the current at $+40$ mV. Block and unblock are not resolved with spermine, but are evident from the transient currents observed with PhTX-343 during the applied step protocol.

the elongated acyl chain (Fig. 1). Moreover, for spermine (and PhTX-343), the fit to our experimental data would indicate a binding site at an electrical distance larger than unity ($\delta = 1.3$, see Discussion). Increasing polyamine concentration did not change the steepness, but shifted $V_{0.5}$ to the right.

Voltage-dependent relief of block at hyperpolarized potentials may indicate punch-through of the blocker to the inside and can be compared for different polyamines by fitting data with a descending Boltzmann function. Although voltage-dependent block and relief of block could be fitted approximately with the appropriate rising or descending single Boltzmann functions with fitting parameters summarized in Table 1, significant deviations at depolarized and hyperpolarized membrane potentials can be observed. The darker solid lines in Fig. 6 represent our attempt to fit the voltage dependence of block by a four-barrier, three-site Eyring rate model, as described in Discussion.

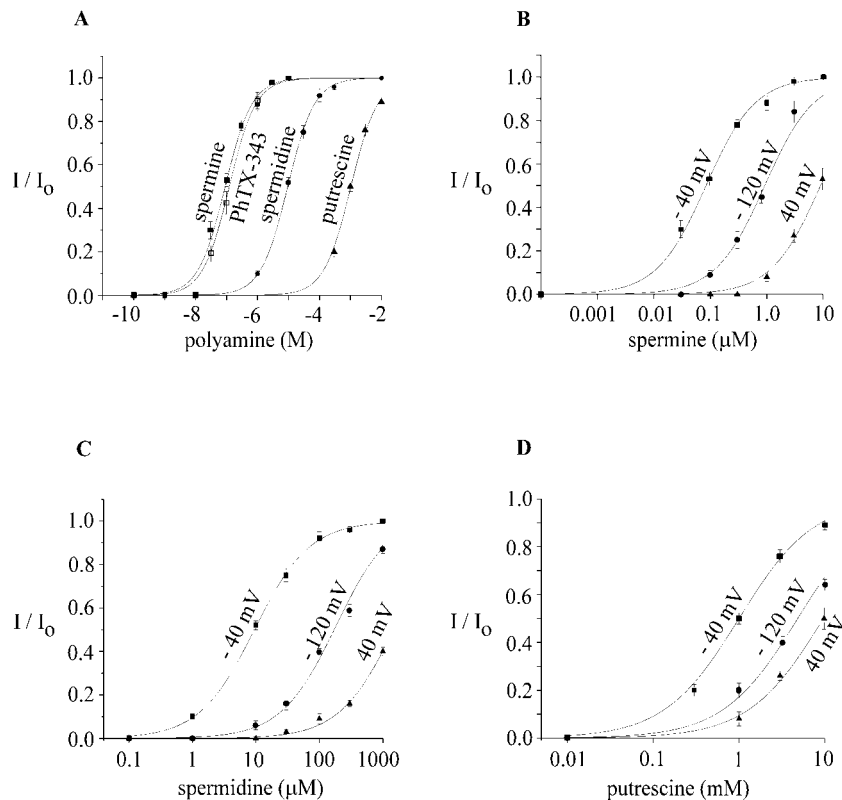


FIGURE 5 Concentration- and voltage-dependent inhibition of MIC current by spermine, spermidine, and putrescine. Current magnitudes were measured using leak-subtracted ramp currents at -120 mV, -40 mV, and $+40$ mV and the data plotted as the ratio of I/I_0 . I_0 represents the current magnitude before application of polyamines and I the current in the presence of polyamines. The data represent mean \pm SD for 10 cells for spermine, spermidine, and putrescine, and five cells for PhTX-343. The effective blocking concentrations for spermine, spermidine, and putrescine were calculated assuming a one binding site model and fitted to $I/I_0 = 1 - (K_{1/2}/[PA] + K_{1/2})$, where $[PA]$ is the extracellular concentration of the polyamine tested and $K_{1/2}$ the blocker concentration that reduces current by 50% at a given membrane potential. (A) Dose-response curves for spermine, philanthotoxin, spermidine, and putrescine at -40 mV. B, C, and D summarize the voltage dependence of the block by spermine, spermidine, and putrescine. All three show the highest affinity for blocking MIC current at -40 mV.

Because of the voltage dependence of polyamine block, higher concentrations were required before block of outward current was observed. Fig. 7 A shows the effect of spermine at $200 \mu\text{M}$, 2 mM, and 20 mM in an RBL cell. At $200 \mu\text{M}$, the inward MIC current was completely blocked, whereas 20 mM was required to block most of the outward current. Block of the outward current is accompanied by changes in the shape of the I/V, thus at high spermine concentrations the outward current became slightly concave, similar to the MIC I/V in presence of millimolar external divalents (Kozak et al., 2002). Ca^{2+} and Mg^{2+} are permeant ions that can carry current through MIC channels (Nadler et al., 2001; Hermosura et al., 2002; Kozak et al., 2002). We attempted to detect inward current carried by spermine at high concentrations, as would be expected for permeant ion

block. Fig. 7 B presents the MIC current I/V curves from panel A on an expanded scale and shows that increasing external spermine concentrations decreased MIC current at both positive and negative potentials; inward current carried by spermine could not be detected. Other investigators have shown that polyamines can act as charge carriers in glutamate channels (Bähring et al., 1997).

Extracellular Mg^{2+} blocks monovalent MIC current in a voltage-dependent manner

Because several types of ion channel exhibit a common site and mechanism of block by Mg^{2+} and polyamines, we compared MIC inhibition by Mg^{2+} and polyamines. In doing so, we hoped to compare block by an approximate

TABLE 1 Analysis of dose-response and voltage-dependent block by polyvalent cations

| | Mg^{2+} | Ca^{2+*} | Putrescine | Spermidine | Spermine | PhTX-343 |
|----------------------------|------------------|-------------------|------------|-----------------|----------|----------|
| Charge (z) | 2 | 2 | 2 | 3 | 4 | 3 |
| $K_{1/2}^\dagger$ | $1 \mu\text{M}$ | $4 \mu\text{M}$ | 1 mM | $9 \mu\text{M}$ | 90 nM | 91 nM |
| k (depol) ‡ | 13.0 | 15.0 | 16.0 | 10.4 | 4.8 | 5.4 |
| $\delta^§$ | 0.85 | 0.81 | 0.78 | 0.8 | 1.3 | 1.3 |
| k (hyperpol) $^\natural$ | 52 | N.D. | 22.4 | 36.8 | 23.2 | 17.6 |

*Data from Kerschbaum and Cahalan, 1998, with Boltzmann fitting redone here for comparison.

† Determined at -40 mV, except for PhTX-343 evaluated at -60 mV.

‡ Steepness of Boltzmann fit for voltage-dependent block (see Fig. 3 legend).

$^\§$ Electrical distance calculated from $k = RT/z\delta F$.

$^\natural$ Steepness of Boltzmann fit for voltage-dependent relief of block.

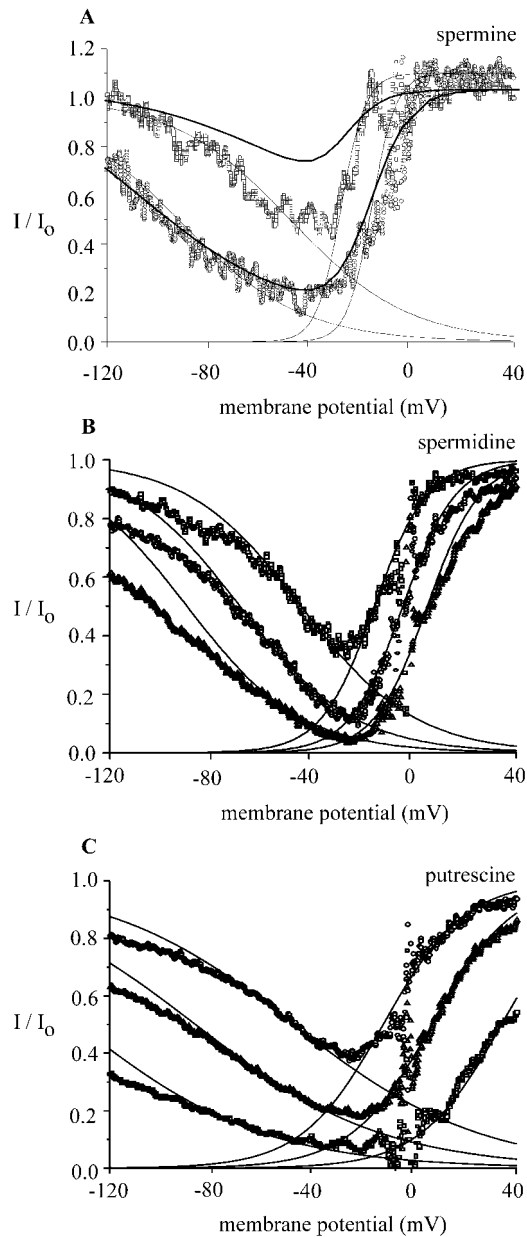


FIGURE 6 Voltage-dependent block of MIC current by spermine (A), spermidine (B), and putrescine (C). Graphs show the ratio of currents (I/I_0) in the presence of polyamines (I) to that in the absence of polyamines (I_0) plotted as a function of the membrane potential. Current ratios for spermine (A), spermidine (B), and putrescine (C) were calculated for experiments shown in Fig. 2. The thin solid lines show fits to a Boltzmann function (see Fig. 3 legend) over a range of depolarized potentials from -30 mV to $+30$ mV, assuming a simple, impermeant block at a site within the membrane electric field; and for relief of block at negative potentials. At depolarized potentials, block was steeply voltage dependent with $z\delta$ products of 5.2 for spermine, 2.4 for spermidine, and 1.6 for putrescine. At hyperpolarized potentials, relief of block was less steep, Boltzmann fits yielding $z\delta$ products of 1.1 for spermine, 0.68 for spermidine, and 1.1 for putrescine. The dark solid lines represent fits of the Eyring model (see Discussion). (A) Increasing the spermine concentration shifts $V_{0.5}$ to the right, from -28 mV (100 nM) to -16 mV (1 μ M). At both concentrations, k is 4.8 mV. For the voltage-dependent relief of block, $V_{0.5}$ is -47.9 mV at 100 nM spermine and -101.6 at 1 μ M spermine; k is 23.2 mV. (B) Spermidine (10 μ M, 30 μ M, and 100

μ M) shifts $V_{0.5}$ from -16 mV to -4.8 mV and $+4.8$ mV, respectively. The slope factor k is 10.4 mV. For relief of block, spermidine (10 μ M, 30 μ M, and 100 μ M) shifts $V_{0.5}$ from -48.0 mV, to -86.9 mV, to -132.8 mV; k is 36.8 mV. (C) Putrescine (1 , 3 , and 10 mM) shifted $V_{0.5}$ from -13 mV to 6 mV to $+34$ mV, respectively. k is 16.0 mV. For relief of block, putrescine shifted $V_{0.5}$ from -44.8 mV, to -68.8 mV, to -89.6 mV; k is 22.4 mV.

point charge (Mg^{2+}) with block by charges that are distributed along the molecule (polyamines). After maximal activation of MIC channels, the cells were exposed to Mg^{2+} at varying concentrations in HEDTA-buffered external solution (Fig. 8). External Mg^{2+} altered the I/V shape of the monovalent current through MIC channels, blocking inward currents preferentially when applied outside in the micromolar range. Fig. 8 B summarizes the inhibitory effect of varying external Mg^{2+} on the current amplitude at -120 , -40 , and $+40$ mV. Consistent with the assumption that one Mg^{2+} ion binds to one site, the data are well fitted to a Langmuir adsorption isotherm ($n = 8$), indicating a high-affinity binding site for externally applied Mg^{2+} ions within the MIC channel. At -40 mV, the monovalent current was blocked most potently with a $K_{1/2}$ of 1 μM Mg^{2+} . At $+40$ mV, the $K_{1/2}$ value was 30 μM Mg^{2+} , and at -120 mV, the $K_{1/2}$ was 3 μM Mg^{2+} . The sensitivity of the monovalent current to block by Mg^{2+} depends strongly upon the membrane potential, with relief of block observed at both hyperpolarized and depolarized potentials, in a manner similar to that described above for polyamines. As also seen with the polyamines (Fig. 5), Mg^{2+} block and unblock equilibrate rapidly on a submillisecond timescale (Fig. 8 C). Mg^{2+} (1 μM) blocked about half of the current at -120 mV, but did not affect the current amplitude at $+40$ mV. The block is too fast to see as a “tail” of current. Because Mg^{2+} block is fast compared with the rate of the voltage ramp, we investigated the voltage dependence of block by analyzing ramp currents. Fig. 8 D illustrates current ratios in the presence and absence of varying Mg^{2+} . Voltage-dependent block by Mg^{2+} suggests that Mg^{2+} from the outside binds at a site most of the way across the membrane electric field. The steepness of block—equivalent to $RT/z\delta F$, where R , T , and F have their usual meanings and δ represents the equivalent electrical distance across the membrane—indicates a $z\sigma$ product of 1.7 ± 0.4 ($n = 3$) for Mg^{2+} . Lines fitted to the data are derived from the four-barrier, three-site Eyring rate model described in Discussion.

Mg^{2+} and spermine block at the single-channel level

To examine the effect of polyvalent cations on the unitary current of MIC channels, we collected single-channel events in the absence and presence of blockers immediately after a single MIC channel became active during whole-cell recording. Representative current traces are illustrated in Fig. 9 for Mg^{2+} and spermine. As previously described, MIC chan-

μM) shifts $V_{0.5}$ from -16 mV to -4.8 mV and $+4.8$ mV, respectively. The slope factor k is 10.4 mV. For relief of block, spermidine (10 μM , 30 μM , and 100 μM) shifts $V_{0.5}$ from -48.0 mV, to -86.9 mV, to -132.8 mV; k is 36.8 mV. (C) Putrescine (1 , 3 , and 10 mM) shifted $V_{0.5}$ from -13 mV to 6 mV to $+34$ mV, respectively. k is 16.0 mV. For relief of block, putrescine shifted $V_{0.5}$ from -44.8 mV, to -68.8 mV, to -89.6 mV; k is 22.4 mV.

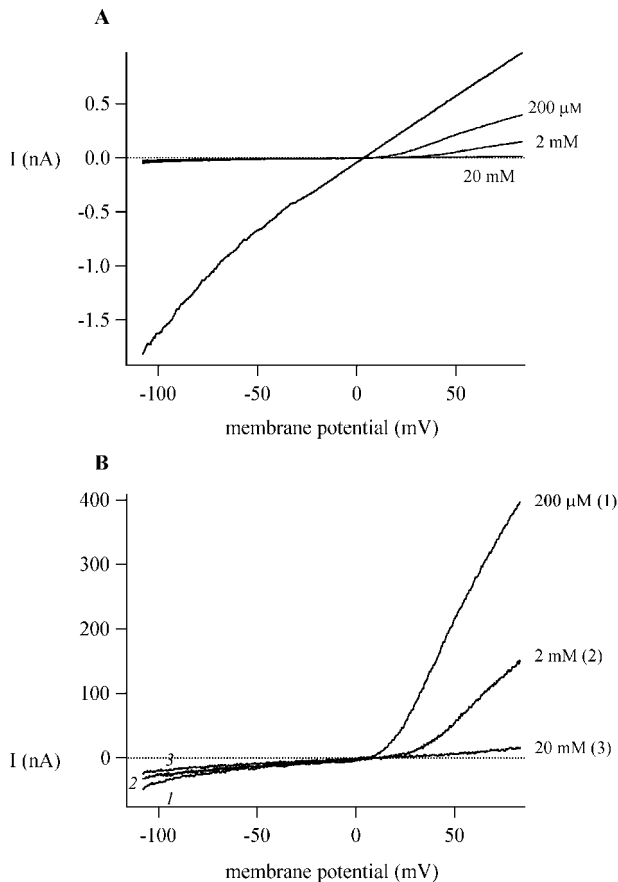


FIGURE 7 High concentrations of external spermine block outward MIC current. (A) I/V relations of MIC current in the presence of 200 μM , 2 mM, and 20 mM spermine in an RBL cell. (B) Traces as in A replotted at magnified scale with the control trace omitted. Increasing concentrations of spermine reduce both the outward and inward current. External solution was 10 HEDTA- Cs^+ . Cs^+ -aspartate concentration was reduced in the external solution containing 20 mM spermine hydrochloride to maintain the osmolarity.

nels activate progressively during whole-cell recording and typically exhibit high open probability (Kerschbaum and Cahalan, 1999). Both Mg^{2+} and spermine, added to the extracellular solution at 0.3 μM –10 μM , produced frequent interruptions in the unitary inward current that represent block of the single channel; increasing concentrations increased the frequency of these flickery block events. Mg^{2+} (1 μM) reduced P_o from 0.94 ± 0.04 ($n = 8$ at -120 mV) in the absence of external polyvalent cations to 0.62 ± 0.16 ($n = 5$); here, changes in P_o represent the reduction in current induced by the blocker, not gating transitions. To compare Mg^{2+} block of macroscopic and single-channel currents, we calculated the apparent dissociation constant from $K_d = k_{\text{off}}/k_{\text{on}}$, where k_{off} and k_{on} are rates of unblock and block and correspond to reciprocals of τ_{closed} and τ_{open} determined from channel lifetime analysis. The K_d for Mg^{2+} block from single-channel analysis was $1.9 \pm 0.5 \mu\text{M}$ ($n = 5$), similar to the $K_{1/2}$ value of 3 μM estimated from Mg^{2+}

block of the macroscopic current at -120 mV (Fig. 8 B). At 10 μM external Mg^{2+} , individual openings and closings were too fast to resolve clearly. Spermine also blocked single MIC channels (Fig. 9 B), causing P_o to decrease to 0.79 ± 0.02 ($n = 4$) and 0.21 ± 0.04 ($n = 5$) at 300 nM and 3 μM , respectively. The corresponding calculated K_d values of 1.1 and 0.8 μM agree well with $K_{1/2}$ of 1 μM determined for spermine block of the macroscopic current (Fig. 5 B). Thus, single-channel analysis reinforces the conclusion that Mg^{2+} or spermine block the channel by binding to a high-affinity site, reducing macroscopic MIC current by flickery block of the unitary current.

Spermine blocks heterologously expressed TRPM7 channels

Several recent studies have indicated that TRPM7 (TRP-PLIK) represents the molecular correlate of the native MIC current (Nadler et al., 2001; Prakriya and Lewis, 2002; Kozak et al., 2002; reviewed in Clapham, 2002; Bakowski and Parekh, 2002). As an additional test, we compared spermine block of TRPM7 current heterologously expressed in CHO cells with native MIC current in RBL cells (Fig. 10, A and B, respectively). Spermine, applied at 200 nM, 2 μM , and 20 μM blocked the TRPM7 monovalent current (in this case carried by Cs^+) in a dose- and voltage-dependent manner. Panel B shows the MIC current block by the same concentrations of spermine under identical conditions in an RBL cell. The voltage dependence of spermine block appears to be similar for both TRPM7 and MIC. A more detailed comparison of the blocking effect of spermine is shown in panel C: the I/Vs in the presence of 2 μM spermine obtained from an RBL cell and a CHO cell transfected with TRPM7 are superimposed and scaled. Although the amount of outward current reduction is slightly less in the TRPM7-transfected cell, the shapes of the I/V in the inward direction are identical, showing that the mechanism of block is the same and providing evidence for a nearly identical binding site within the pores of native MIC and expressed TRPM7 channels.

DISCUSSION

Defining a site within the MIC channel

In the present study, we have characterized a binding site within MIC channels that interacts with polyvalent cations including polyamines and Mg^{2+} from the outside. With single-channel resolution, block by spermine or Mg^{2+} can be directly observed as interruptions of the long-duration openings that are characteristic of MIC channels (Fig. 9). Such flickery block events are consistent with entry of blocker into the channel, disrupting the flow of monovalent cations by occlusion. The site of block is within the electric field of the membrane, accessible from the outside but not

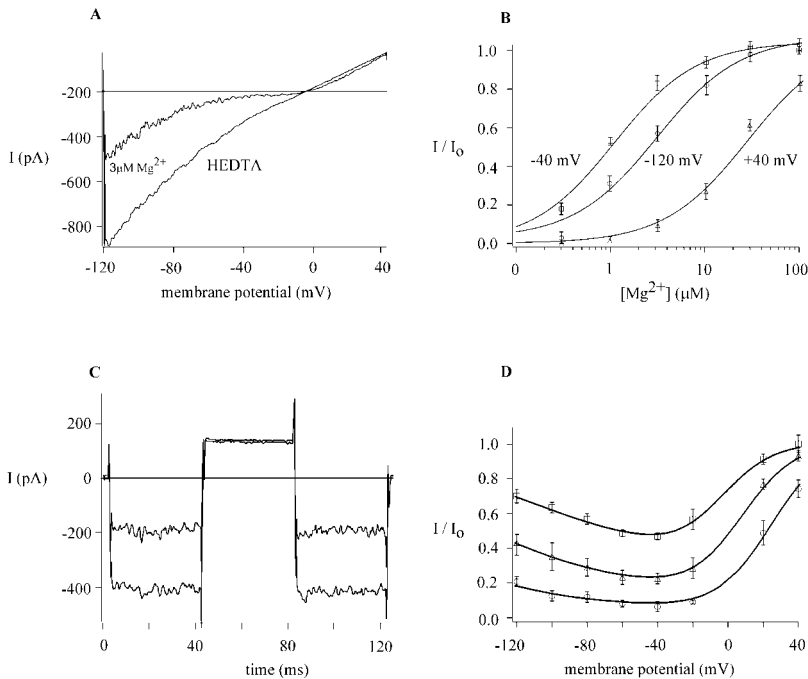


FIGURE 8 Voltage- and concentration-dependent block of monovalent current through MIC channels by $[\text{Mg}^{2+}]_o$. (A) I/V curves in the absence and presence of $3 \mu\text{M}$ external Mg^{2+} . (B) The concentration dependence of block obtained by fitting the dose-response relations (mean \pm SD, $n =$ eight cells) at -120 mV , -40 mV , and $+40 \text{ mV}$; corresponding $K_{1/2}$ values are $3 \mu\text{M}$, $1 \mu\text{M}$, and $30 \mu\text{M}$, respectively. (C) Fast kinetics of block at -40 mV and relief of block at $+40 \text{ mV}$. (D) Voltage-dependent block of monovalent current with $1 \mu\text{M}$ Mg^{2+} (squares), $3 \mu\text{M}$ Mg^{2+} (triangles), and $10 \mu\text{M}$ Mg^{2+} (circles). The data points represent the unblocked fraction of the Na^+ current at each potential. Note that the relief of block at hyperpolarized potentials wanes with increasing $[\text{Mg}^{2+}]_o$. Smooth curves represent fits from the Eyring rate model.

the inside and yet closer to the cytoplasm in terms of equivalent electrical distance. For block by external Mg^{2+} , the simplest interpretation is that Mg^{2+} moves $\sim 85\%$ down the electric field where it binds tightly enough to block Na^+ current. This equivalent electrical distance is similar to that previously determined for Ca^{2+} ions blocking monovalent current from the outside, indicating a common high-affinity binding site for Mg^{2+} and Ca^{2+} (Kerschbaum and Cahalan, 1998).

The externally accessible site for Mg^{2+} (or Ca^{2+}) is distinct from the internal Mg^{2+} site that controls current development during whole-cell recording. The channel opens when the cytoplasm is depleted of Mg^{2+} during whole-cell recording and dialysis. Mg^{2+} in the high micromolar to low millimolar range blocks without affecting the I/V shape. In cells with preactivated MIC channels, the block by internal Mg^{2+} is slow to equilibrate, taking longer than expected for Mg^{2+} to diffuse into the cell. This may indicate that Mg^{2+} does not exert a direct effect upon the channel by simple block (Kozak et al., 2002). The internal site for Mg^{2+} block remains uncertain, but is certainly distinct from the externally accessible Mg^{2+} or polyamine block site.

Block by external polyamines, like that of external Mg^{2+} , is voltage-dependent, indicating external access to a site within the electric field of the membrane (Figs. 2–5). Charges are distributed along the alkyl chain of polyamines, and the sensitivity to membrane potential parallels the number of charges. Table 1 summarizes $K_{1/2}$ values measured at -40 mV and the steepness factor k , determined by fitting ratio I/V curves. Surprisingly, the longest polyamines tested, spermine and PhTX-343, each blocked with

a steepness that would indicate a fractional distance across the electric field, δ , of >1 , similar to steeply voltage-dependent polyamine block reported for inward rectifier potassium channels (Fakler et al., 1995; Lopatin et al., 1994; Lopatin et al., 1995; Pearson and Nichols, 1998). These results point to multiple molecules simultaneously being able to block within the electric field of the channel or to a coupled movement of the blocking ion and the permeant ion through the ion channel (Lopatin et al., 1994, 1995; Fakler et al., 1995; Oliver et al., 1998; Pearson and Nichols, 1998; Oliver et al., 2000). Thus, spermine could interact with its positive charges simultaneously at different binding sites of the MIC channel and sweep out associated permeating monovalent cations.

The relief of Mg^{2+} block that occurs at very hyperpolarized membrane potentials may be accounted for by “punch-through,” in which hyperpolarization provides the sparingly permeant Mg^{2+} ion with sufficient energy to “knock off” Mg^{2+} from the binding site, enabling Na^+ to carry current again. Block by polyamines can also be relieved by membrane hyperpolarization, consistent with a small but finite permeability through the channel by all compounds studied. Ca^{2+} and Mg^{2+} currents through MIC and expressed TRPM7 channels have been directly measured (Nadler et al., 2001; Hermosura et al., 2002; Kozak et al., 2002), and thus it is not surprising that Mg^{2+} can act as a permeant blocker.

Modeling the block

The simplest model for a permeant blocker represents a binding site within the channel pore that can be occupied

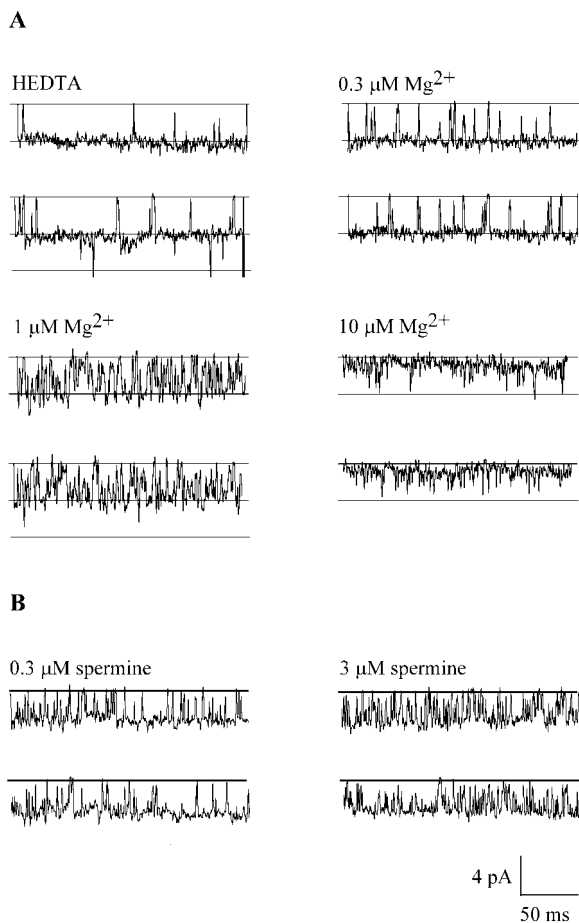


FIGURE 9 $[Mg^{2+}]_o$ or spermine block MIC single channels. Single channel currents carried by Na^+ recorded at -120 mV during whole-cell recording near the onset of MIC current development. The data were filtered at 700 Hz and sampled at 10 kHz. Most of the records display activity of a single channel. (A) Representative current traces recorded either in HEDTA-buffered, Mg^{2+} -free external solution (*top left*) or in solutions buffered to indicated free Mg^{2+} concentrations. Brief openings of a second channel can be seen in the traces on the left. (B) Representative single-channel currents with 0.3 and 3 μM spermine.

by a single permeant ion or by a blocking ion, corresponding to a two-barrier, one-binding site model of the type originally described by Woodhull (1973):



in which O represents the open channel, B_{out} the blocker on the outside of the membrane, and B_{in} the blocker on the inside. Although attractive in terms of simplicity, this model did not adequately fit our data on polyamine or Mg^{2+} block, failing to predict the correct current ratios at varying concentrations. The MIC channel is permeable to Na^+ and other monovalent cations in the absence of divalent cations, binds Ca^{2+} or Mg^{2+} with high affinity in the low μM range, and is permeable to Ca^{2+} ions when these divalent ions are present in the mM range, properties that are reminiscent of voltage-gated Ca^{2+} channels. To simulate current-voltage re-

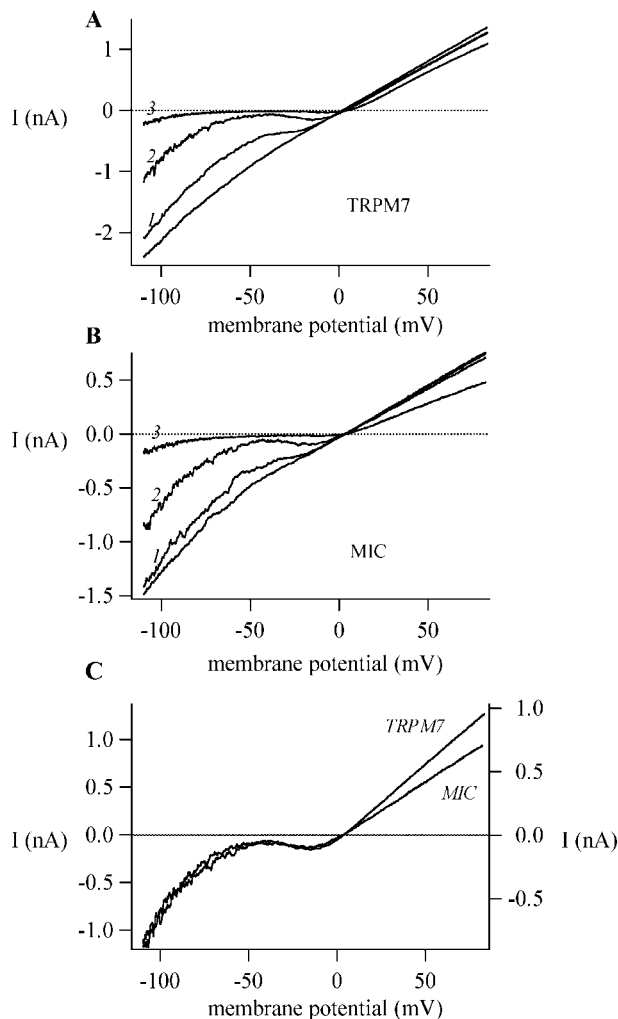
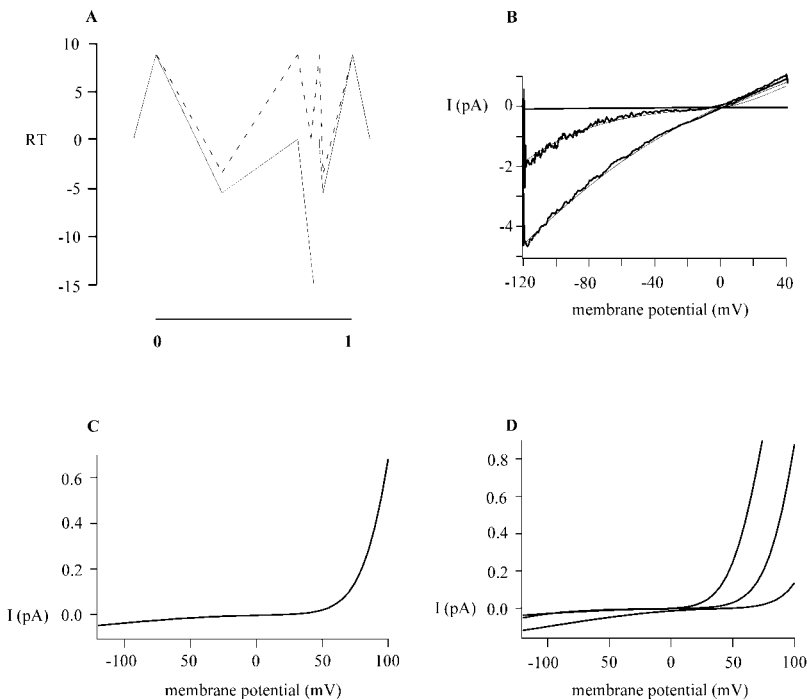


FIGURE 10 Spermine blocks heterologously expressed TRPM7 current. (A) TRPM7-transfected CHO cell. Increasing concentrations of spermine block the current in the absence of external divalents (10 HEDTA- Cs^+). Traces 1, 2, and 3 represent I/Vs in 200 nM, 2 μM , and 20 μM spermine, respectively. (B) Spermine block of the native MIC current in an RBL cell under the same conditions as A. (C) Traces 2 from panels A and B superimposed for comparison.

lationships and voltage-dependent block of MIC current by extracellular polyvalent cations, we employed an Eyring rate model similar to one used to describe ion permeation in Ca^{2+} channels (discussed in McCleskey, 1999), with a single high-affinity site for binding within the electric field by polyamines or Mg^{2+} , flanked by two low-affinity sites. The cation pathway through the channel is depicted as a sequential series of four barriers and three wells, allowing multiple occupancy of the channel by more than one ion.

Starting with Na^+ , we established a set of barriers and wells that gave approximately the right I/V shape and single-channel conductance values (Fig. 11 A, *dashed lines*). Outer and inner barriers were set to 8.7 RT, corresponding to diffusion-limited access to the pore, and well depths were adjusted empirically to produce the resulting I/V curve in



current, and a small inward current carried by Mg^{2+} . Concentrations used: $[\text{Na}^+]_e = [\text{Na}^+]_i = 150 \text{ mM}$; $[\text{Mg}^{2+}]_e = 3 \text{ mM}$; $[\text{Mg}^{2+}]_i = 0$. (D) I/V curves calculated for 0.2, 2, and 20 mM spermine with symmetrical 150 mM $[\text{Na}^+]_i$.

Fig. 11 B. The model produces the characteristic weak inward rectification of MIC current in symmetrical Na^+ and zero divalent, with a single-channel current of 4.5 pA at -120 mV , in accord with direct measurement (Kerschbaum and Cahalan, 1999). Next, based on the steepness and potency of block by spermine or Mg^{2+} at depolarized potentials, we incorporated a high-affinity binding site most of the way toward the inner surface of the membrane. In physical terms, the deep energy well could be provided by fixed negative charges within the pore, such as glutamate residues that are present in the putative pore region of TRPM7. The well depth was calculated from the apparent dissociation constant by $G = -RT \ln(K_d)$, where $K_d = k_{\text{off}}/k_{\text{on}}$. Based on experimental data, we postulated a high-affinity binding site for Mg^{2+} of -15 RT (which represents a K_d value of $0.8 \mu\text{M}$ at -40 mV) at a δ of 0.80. The position and well depth of the high-affinity site and the location of the flanking low-affinity binding sites as well as magnitude of the surface potential were then fine-tuned in an effort to mimic the available experimental data. The final energy profile for Mg^{2+} is shown by the solid lines in Fig. 11 A. Calculated I/V curves at $3 \mu\text{M}$ and 3 mM Mg^{2+} are illustrated in Fig. 11, B and C, respectively. Note that the model provides an accurate fit to the shape of the I/V curve at $3 \mu\text{M}$ Mg^{2+} , a concentration at which Mg^{2+} acts as a voltage-dependent blocker whereas Na^+ carries the current and also reproduces the characteristic outwardly rectifying MIC I/V shape at 3 mM Mg^{2+} , a concentration at which

FIGURE 11 Four-barrier, three-site model for permeation and block in the MIC channel. The model allows adjustment of Gibbs free energy values (G , indicated as multiples of thermal energy) of barrier and wells for each ionic species relative to the bulk solution, the location of the binding site within the electrical field, magnitude of the surface potential, and extra- and intracellular monovalent and divalent cations at varying concentrations. (A) Energy profile for Na^+ (dashed lines) and Mg^{2+} (solid lines). For Na^+ , the well depths in multiples of RT are -3.15 , 0 , and 3.15 ; barrier heights are 8.7 . Parameters for Mg^{2+} include a high-affinity binding site of -15 RT (corresponding to a K_d of $0.8 \mu\text{M}$) at an electrical distance δ of 0.8 , and two low-affinity binding sites of -5.5 RT at δ values of 0.35 and 0.85 . In addition, an internal surface potential of 30 mV was required for the best fit. For spermine (not shown), the parameters include well depths of -5.5 , -15 , and -5.5 RT located at δ values of 0.05 , 0.8 , and 0.95 from the outside. Inner and outer surface potentials of 30 mV and 10 mV were also included. We did not include a factor for repulsive interactions between cations at adjacent sites. (B) Predicted and observed I/V relations in the absence and presence of $3 \mu\text{M}$ Mg^{2+} . Concentrations used: $[\text{Na}^+]_e = [\text{Na}^+]_i = 150 \text{ mM}$; $[\text{Mg}^{2+}]_e = 3 \mu\text{M}$; $[\text{Mg}^{2+}]_i = 0$. Noisy traces represent data replicated from Fig. 8 A for comparison. (C) Predicted I/V relations at 3 mM Mg^{2+} showing the characteristic outward rectification of MIC

Mg^{2+} carries the inward current. At millimolar levels of Mg^{2+} , the small predicted Mg^{2+} current is 1% of the corresponding predicted Na^+ current in the absence of divalent. This predicted Mg^{2+} current is in accord with a small measured Mg^{2+} current (Kozak et al., 2002). Finally, the model also provides an excellent fit to I/V ratios at varying concentrations of external Mg^{2+} , as shown in Fig. 8 D, indicating that the model adequately accounts for characteristics of voltage-dependent Mg^{2+} block and relief of block at more hyperpolarized membrane potentials. At millimolar concentrations, internal Mg^{2+} inhibits MIC current without altering the shape of the I/V curve (Kozak et al., 2002). Apparently, Mg^{2+} is unable to access the pore from the inside. For spermine, a well depth of -15 RT and δ of 0.8 also worked quite well in predicting voltage-dependent block at single concentrations (Fig. 6 A), and predicted block of outward currents in the correct range of concentrations (cf. Figs. 11 D and 7 A), but did not work accurately at spermine concentrations below $1 \mu\text{M}$ (note deviations in Fig. 6 A). In addition, the model predicts an inward spermine current at high concentrations that could not be detected (Fig. 7 B), and predicts inward rectification induced by internal spermine at concentrations in the high micromolar range, an effect that also was not observed. To summarize, the Eyring rate approach yielded a more accurate fit to data for block by external Mg^{2+} than for spermine. This difference may be due to the distribution of charge along the spermine molecule that permits spermine to interact

TABLE 2 Comparison of pore sizes using permeant ions and polyamines as probes

| | MIC | K _{IR} | Na ⁺ | CNG | GluR |
|-----------------------------------|------------------|------------------|----------------------|------------------|--|
| Ion selectivity | Mono-, divalents | K ⁺ | Na ⁺ | Mono-, divalents | Mono-, divalents |
| Pore size (from permeant ions) | 5.8 Å* | 3 Å | 3 × 5 Å [†] | ~5 Å | 5.5 Å [‡] , ~7 Å [§] |
| Permeant block by spermine | Yes | Yes [¶] | Yes [¶] | Yes** | Yes ^{††} |
| Permeant block by PhTX | Yes | No | ND | ND | Yes ^{‡‡} |
| Pore size (from blockers) | 7.4 Å | 4.6 Å | 4.6 Å | 4.6 Å | 7.4 Å |

*Kerschbaum and Cahalan, 1998.

[†]Hille, 2001.

[‡]Wollmuth et al., 1996.

[§]Burnashev et al., 1996.

[¶]Guo and Lu, 2000.

^{||}Huang and Moczydlowski, 2001.

**Lu and Ding, 1999.

^{††}Bähring et al., 1997.

^{‡‡}Bähring and Mayer, 1998.

ND, not determined.

simultaneously with more than one site or to interact with permeant ions, features not incorporated in our model. Further studies on ion permeation and block are needed to investigate the asymmetry of the MIC channel.

Polyamines block native MIC and expressed TRPM7 channels comparably

We compared I/V shapes of native MIC currents and TRPM7-induced currents in CHO cells, and used spermine as a sensitive probe for the pore. In other channel types, a small change in structure can be detected by channel blockers. For example, a single amino acid difference in the pore region of the Na⁺ channel can dramatically alter spermine block (DEKA versus DEAA) (Huang and Moczydlowski, 2001). Our data are consistent with previous conclusions that the native MIC current passes through channels composed of TRPM7 subunits.

Comparing permeation and pores of MIC/TRPM7 and other channels

Traditionally, the minimal pore size of an ion channel can be estimated by the largest permeant ion that can carry a measurable current (Hille, 2001). In previous work, we measured the ability of several different organic cations to carry current through the MIC channel. In these studies, MIC current was unmasked by withdrawal of internal Mg²⁺ and erroneously attributed to the CRAC channel. Nevertheless, the results apply to the MIC channel and provide an estimated pore diameter of ~5.8 Å; even tetramethylammonium with a diameter of 5.5 Å is a permeant ion (Kerschbaum and Cahalan, 1998). This procedure for determining the pore diameter excludes sparingly permeant compounds whose current is not resolvable (Burnashev et al., 1996). Alternatively, the minimal pore diameter of ion channels can be estimated from the size of permeant blockers. Spermine,

the largest of the three cytoplasmic polyamines tested with a length of 20 Å and a diameter of ~4.6 Å, behaved as a permeant blocker and would be able to fit easily through a pore of 6 Å. Surprisingly, even PhTX-343 exhibited punch-through, indicating that the pore can accommodate a molecule of 7.4 Å in diameter. Similar discrepancies between pore size estimated from permeant ions and permeant blockers have been documented for other channel types. Spermine is a permeant blocker of the K_{IR} channel and the voltage-gated Na⁺ channel with estimated pore sizes of 3 Å and 3 × 5 Å based on the largest permeant ions (Guo and Lu, 2000b; Huang and Moczydlowski, 2001; Hille, 2001). The GluR6 channel is larger; spermine can carry measurable current, and PhTX exerts permeant block (Bähring et al., 1997; Bähring and Mayer, 1998). Several properties of polyamine block in different channel types are compared in Table 2; permeant blockers generally give a larger estimate of the pore size than permeant ions that carry measurable current.

We thank Lu Forrest for excellent assistance in cell culture. We are grateful to David Clapham and Loren Runnels for providing the TRPM7 clone. Ted Begenisich graciously provided us with the four-barrier, three-site Eyring rate theory computer program, which we adapted for the model calculations. We also thank Heike Wulff and Jim Hall for valuable discussion.

This work was supported by grants from the Austrian Science Fund (13395-MOB to H.H.K.) and by National Institutes of Health grant NS14609 (to M.D.C.).

REFERENCES

- Araneda, R. C., J. Y. Lan, X. Zheng, R. S. Zukin, and M. V. Bennett. 1999. Spermine and arcaine block and permeate N-methyl-D-aspartate receptor channels. *Biophys. J.* 76:2899–2911.
- Bähring, R., D. Bowie, M. Benveniste, and M. L. Mayer. 1997. Permeation and block of rat GluR6 glutamate receptor channels by internal and external polyamines. *J. Physiol. (Lond.)* 502:575–589.

- Bähring, R., and M. L. Mayer. 1998. An analysis of philanthotoxin block for recombinant rat GluR6(Q) glutamate receptor channels. *J. Physiol. (Lond.)*. 509:635–650.
- Bakowski, D., and A. B. Parekh. 2002. Permeation through store-operated CRAC channels in divalent-free solutions: potential problems and implications for putative CRAC channel genes. *Cell Calcium*. 32:379–391.
- Bers, D. M., C. W. Patton, and R. Nuccitelli. 1994. A practical guide to the preparation of Ca^{2+} buffers. *Methods Cell Biol.* 40:3–29.
- Braun, F. J., L. M. Broad, D. L. Armstrong, and J. W. Putney Jr. 2001. Stable activation of single Ca^{2+} release-activated Ca^{2+} channels in divalent cation-free solutions. *J. Biol. Chem.* 276:10663–1070.
- Burnashev, N., A. Villaruel, and B. Sakmann. 1996. Dimensions and ion selectivity of recombinant AMPA and kainate receptor channels and their dependence on Q/R site residues. *J. Physiol. (Lond.)*. 496:165–173.
- Cahalan, M. D., H. Wulff, and K. G. Chandy. 2001. Molecular properties and physiological roles of ion channels in T lymphocytes. *J. Clin. Immunol.* 21:235–252.
- Clapham, D. E. 2002. Sorting out MIC, TRP, and CRAC Ion Channels. *J. Gen. Physiol.* 120:217–220.
- Eldefrawi, A. T., M. E. Eldefrawi, K. Konno, N. A. Mansour, K. Nakanishi, E. Oltz, and P. N. Usherwood. 1988. Structure and synthesis of a potent glutamate receptor antagonist in wasp venom. *Proc. Natl. Acad. Sci. USA*. 85:4910–4913.
- Fakler, B., U. Brandle, E. Glowatzki, S. Weidemann, H. P. Zenner, and J. P. Ruppersberg. 1995. Strong voltage-dependent inward rectification of inward rectifier K^{+} channels is caused by intracellular spermine. *Cell*. 80:149–154.
- Fomina, A. F., C. M. Fanger, J. A. Kozak, and M. D. Cahalan. 2000. Single channel properties and regulated expression of Ca^{2+} release-activated Ca^{2+} (CRAC) channels in human T cells. *J. Cell. Biol.* 150:1435–1444.
- Guo, D., and Z. Lu. 2000a. Mechanism of cGMP-gated channel block by intracellular polyamines. *J. Gen. Physiol.* 115:783–798.
- Guo, D., and Z. Lu. 2000b. Mechanism of IRK1 channel block by intracellular polyamines. *J. Gen. Physiol.* 115:799–814.
- Hamill, O. P., A. Marty, E. Neher, B. Sakmann, and F. J. Sigworth. 1981. Improved patch-clamp techniques for high-resolution current recording from cells and cell-free membrane patches. *Pflügers Arch.* 391:85–100.
- Hermosura, M. C., M. K. Monteilh-Zoller, A. M. Scharenberg, R. Penner, and A. Fleig. 2002. Dissociation of the store-operated calcium current I(CRAC) and the Mg-nucleotide-regulated metal ion current MagNum. *J. Physiol. (Lond.)*. 539:445–458.
- Hille, B. 2001. Ion Channels of Excitable Membranes, 3rd ed. Sinauer Associates, Sunderland, MA.
- Huang, C. J., and E. Moczydlowski. 2001. Cytoplasmic polyamines as permeant blockers and modulators of the voltage-gated sodium channel. *Biophys. J.* 80:1262–1279.
- Kerschbaum, H. H., and M. D. Cahalan. 1998. Monovalent permeability, rectification, and ionic block of store-operated calcium channels in Jurkat T lymphocytes. *J. Gen. Physiol.* 111:521–537.
- Kerschbaum, H. H., and M. D. Cahalan. 1999. Single channel recording of a store-operated Ca^{2+} channel in Jurkat T lymphocytes. *Science*. 283:836–839.
- Kozak, J. A., H. H. Kerschbaum, and M. D. Cahalan. 2002. Distinct properties of CRAC and MIC channels in RBL cells. *J. Gen. Physiol.* 120:221–235.
- Lepple-Wienhues, A., and M. D. Cahalan. 1996. Conductance and permeation of monovalent cations through depletion-activated Ca^{2+} channels (ICRAC) in Jurkat T cells. *Biophys. J.* 71:787–794.
- Lopatin, A. N., E. N. Makhina, and C. G. Nichols. 1994. Potassium channel block by cytoplasmic polyamines as the mechanism of intrinsic rectification. *Nature*. 372:366–369.
- Lopatin, A. N., E. N. Makhina, and C. G. Nichols. 1995. The mechanism of inward rectification of potassium channels: “long-pore plugging” by cytoplasmic polyamines. *J. Gen. Physiol.* 106:923–955.
- Lu, Z., and L. Ding. 1999. Blockade of a retinal cGMP-gated channel by polyamines. *J. Gen. Physiol.* 113:35–43.
- McCleskey, E. 1999. Calcium channel permeation: a field in flux. *J. Gen. Physiol.* 113:765–772.
- Nadler, M. J., M. C. Hermosura, K. Inabe, A. L. Perraud, Q. Zhu, A. J. Stokes, T. Kurosaki, J. P. Kinet, R. Penner, A. M. Scharenberg, and A. Fleig. 2001. LTRPC7 is a Mg-ATP-regulated divalent cation channel required for cell viability. *Nature*. 411:590–595.
- Oliver, D., H. Hahn, C. Antz, J. P. Ruppersberg, and B. Fakler. 1998. Interaction of permeant and blocking ions in cloned inward-rectifier K^{+} channels. *Biophys. J.* 74:2318–2326.
- Oliver, D., T. Baukrowitz, and B. Fakler. 2000. Polyamines as gating molecules of inward-rectifier K^{+} channels. *Eur. J. Biochem.* 267:5824–5829.
- Pearson, W. L., and C. G. Nichols. 1998. Block of the Kir2.1 channel pore by alkylamine analogues of endogenous polyamines. *J. Gen. Physiol.* 112:351–363.
- Prakriya, M., and R. S. Lewis. 2002. Separation and characterization of currents through store-operated CRAC channels and Mg^{2+} -inhibited cation (MIC) channels. *J. Gen. Physiol.* 119:487–507.
- Runnels, L. W., L. Yue, and D. E. Clapham. 2001. TRP-PLIK, a bifunctional protein with kinase and ion channel activities. *Science*. 291:1043–1047.
- Wollmuth, L. P., T. Kuner, P. H. Seeburg, and B. Sakmann. 1996. Differential contribution of the NR1- and NR2A-subunits to the selectivity filter of recombinant NMDA receptor channels. *J. Physiol. (Lond.)*. 491:779–797.
- Woodhull, A. M. 1973. Ionic blockage of sodium channels in nerve. *J. Gen. Physiol.* 61:687–708.